# Solubility of Au and Ir in Carbonate Melts: Implications for the Precious Metal Potential of Carbonatites and Mantle Metasomatism.

by

Robin Wolf

# LIST OF FIGURES

*Number* *Page*

TABLE OF CONTENTS

# LIST OF TABLES

*Number* *Page*

# Solubility of Au and Ir in Carbonate Melts: Implications for the Precious Metal Potential of Carbonatites and Mantle Metasomatism.


## Abstract

Few studies have examined the precious metals potential of carbonatites. As a first step in beginning to understand the behaviour of precious metals in carbonatites, this study examined the solubility of Au and Ir in simple carbonate melts. Preliminary experiments looked at the solubility of Pt in carbonate melts using a piston cylinder apparatus. This approach was abandoned due to surface Pt contamination and textural heterogeneity issues. The second round of experiments was done at 0.1 MPa using vacuum-sealed silica ampoules containing gold capsules and different metal oxide buffers. Au and Ir solubilities were analyzed by Standard Addition Solution ICP-MS. Au solubility was determined to be linearly dependent on the $fO_2$ - as oxygen fugacity decreases, Au solubility also decreases. The 0.28 slope of the solubility vs. log $fO_2$ trend line showed that Au probably dissolves as $Au^{+1}$ and the dissolved metal species in the carbonate melt was assumed to be $Au_2O$. Comparing data with Borisov and Palme (1996), it is clear that Au solubility in carbonate melts is two orders of magnitude higher than in silicate melts. However, the experimental results at log $fO_2$ -6.7 were anomalously low compared to the predicted value from the slope line. SEM investigation revealed that a fragment of the quenched melt product appeared to have remained solid. In contrast to the Au results, Ir solubility results are inconclusive. There appears to be no relationship between Ir solubility and log $fO_2$, but this may be due to the detection limitations of the ICP-MS.

## Introduction

The precious metals comprise the highly siderophile elements (HSEs), which have very high metal/melt partition coefficients (>$10^4$). Knowledge of the behaviour of HSEs in melts is important in helping to understand mantle/core segregation, mantle geochemistry and associated processes. Historically, the solubility behaviour of HSEs has been difficult to characterize, owing to the extremely low concentrations in the melt and the limitations of analytical methods (Ertel et al., 2008). Laser Ablation Inductively Coupled Plasma Mass Spectrometry (LA-ICPMS) has become an invaluable analytical method for HSE solubility analysis, and has greatly improved the accuracy and detection limits of HSE concentrations (Ertel et al., 2008). To date most studies have investigated the solubility of PGEs, Au and Re in silicate melts (i.e. Borisov & Palme, 1996; Ertel et al, 2001; Ertel et al, 1999). However, there have been few studies on the geochemical behaviour of PGEs and Au in carbonatites (Xu et al., 2003).

Carbonatites are rare magmatic rocks derived from the mantle and contain more than 50% carbonates (Xu et al., 2008; Fischer et al., 2009). Because they are mantle derived, they are useful for investigating mantle metasomatism and melt evolution. As shown in Figure 1, carbonated peridotites can produce carbonate melts at great depths in the mantle, such that carbonate melt can exist when silicate melts do not. Wallace and Green (1988) found that carbonate-rich fluids act as metasomatic agents in the mantle – they are able to mobilize trace elements. While it is known that carbonate melts can effectively mobilize rare earth elements (REE) and large-ion lithophile elements (LILE) (Srivastava, 1997; Wallace and Green, 1998), their impact on HSEs is unknown. Thus, a

first step in beginning to understand the behaviour of HSEs in carbonatites is to examine how HSEs dissolve in simple carbonate melts.

Currently, there is little to no data on the PGE or Au content of carbonatites. Xu et al. (2008) examined the concentrations of PGEs in 29 intrusive and extrusive carbonatites across China. They found that all samples had low magmatic sulphide abundances and low total PGE concentrations (0.07–2.5 ppb). They hypothesized that the low PGE abundances could be related to early sulfide saturation and the formation of an immiscible sulfide melt, causing a depletion of PGE concentration in the carbonatites. Xu et al. (2003) also conducted a preliminary study on the PGE concentration of carbonatites from South West China, but the digestion method for sample dissolution was unsuitable for PGE poor carbonatites, and thus their results are unreliable.

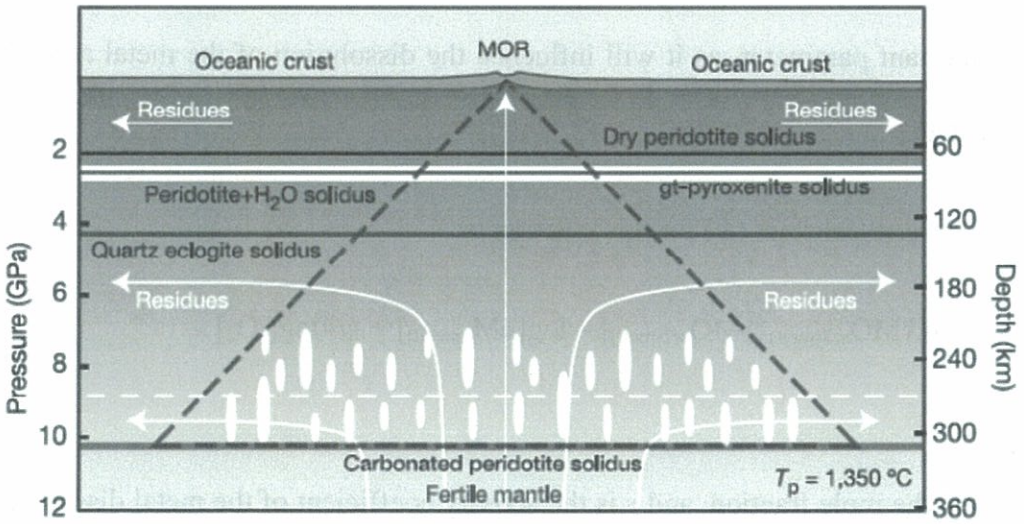


*Figure 1: Solidus pressure for 1350 C mantle potential temperature. The white blebs are seismic anomalies, which indicate melting (Dasgupta and Hirschmann, 2006).*

The determination of the solubility of HSEs in carbonate melts will help in better understanding how or if these elements can be mobilized by such melts. In order to investigate the behaviour of HSEs in carbonatites a number of experiments were performed that examined the solubility of Pt, Au and Ir in carbonate melts.

## Thermodynamic background

To understand how precious metals are thought to dissolve in melts, it is necessary to examine the thermodynamics of the reaction between them. The following reaction shows how a siderophile element partitions between a melt and metal:

$$M_{(metal)} + x/4O_2 \leftarrow \rightarrow MO_{x/2(melt)} \quad (1)$$

where x = valence of dissolved metal species. It is clear then, that the $fO_2$ of the reaction is an important parameter, as it will influence the dissolution of the metal and affect its valence state.

The equilibrium constant ($K$) for this reaction is:

$$\log K = \log[XMO_{x/2(melt)} * \gamma MO_{x/2(melt)}] - \log[aM_{\{metal)}] + x/4\log[fO_2] \quad (2)$$

where $X$ is the mole fraction, and $\gamma$ is the activity coefficient of the metal dissolved in the melt and $a$ is the activity of the metal in the metal phase. Since it is assumed that saturation in the pure phase occurs, $aM = 1$.

Equation 2 can be rearranged to give the solubility of the metal oxide:

$$\log [X\mathrm{MO}_{x/2(\mathrm{melt})}] = x/4\log[fO_2] + C \quad (3)$$

Henry's law applies as it is assumed that the concentration of the metal dissolved in the melt is low enough at saturation that essentially $\gamma\mathrm{MO}_{x/2(\mathrm{melt})}$ = Constant ($C$). Equation (3) shows that the solubility of the metal of interest should proportionally increase at a rate of x/4 as oxygen fugacity increases – thus the oxidation state of the metal in the melt is important.

## Experiment Overview and Procedures

### Overview

As the purpose of this study was to determine the solubility of the precious metal of interest, the experimental methods used attempted to equilibrate molten carbonate with the precious metal at a controlled $fO_2$ (or at a $fO_2$ that could be estimated after). Two experimental procedures were used in this study.

The first experiments looked at the solubility of Pt in carbonate melts. High-pressure piston cylinder experiments were conducted with graphite capsules containing the melt, Pt and magnetite. The $fO_2$ was estimated from the Fe content of the added Pt. While it is acceptable to estimate $fO_2$ in this fashion, the $fO_2$ can proceed to very low values, and can result in unmeasurable Pt solubilities. This occurred with the first two runs, so in an attempt to prevent such low $fO_2$, the graphite capsules were sealed in Pt capsules, and one experiment used a magnetite capsule instead of graphite. However, the

magnetite capsule leaked, and this approach was abandoned. Due to difficulties in sample analysis with the piston cylinder experiments, another approach was sought.

The second round of experiments was done at 0.1 MPa using vacuum-sealed silica ampoules containing gold capsules and different metal oxide buffers. These experiments looked at the solubility of Au, but Ir wires were also added to measure its solubility. This could be done as Ir and Au are mutually insoluble, and so their activities remain near 1.

The following sections describe in detail the experimental procedures used.

**Piston Cylinder Experiments**

A simple melt composition of $CaCO_3$ and $Na_2CO_3$ was chosen for initial experimentation and exploration. Based on the paper by Wallace & Green (2006) a melt of 4:1 wt % $CaCO_3$:$Na_2CO_3$ was made using high purity powders.

A number of steps were taken to prepare the assembly for high pressure and temperature piston cylinder experiments. A mixture of 0.5 mg of Pt powder and 2 mg of magnetite (Mt) powder was put in a 7 mm graphite capsule, then 7 mg of the prepared melt was put in. For three of the experiments the graphite capsule was placed in a Pt capsule and then sealed. For the magnetite capsule experiment, a mixture of hematite and Pt was added. The graphite capsule was then placed in a magnesia filler piece sleeve. An additional magnesia filler piece was placed on top. The filler pieces were then inserted in to a ½" graphite furnace, which was then placed in a $BaCO_3$ sleeve and wrapped in Pb foil. The sample was then put in the pressure vessel, and a standard procedure was

followed to set up the piston cylinder apparatus. See the schematic in Figures 2 and 3 for visual representations of the assembly.

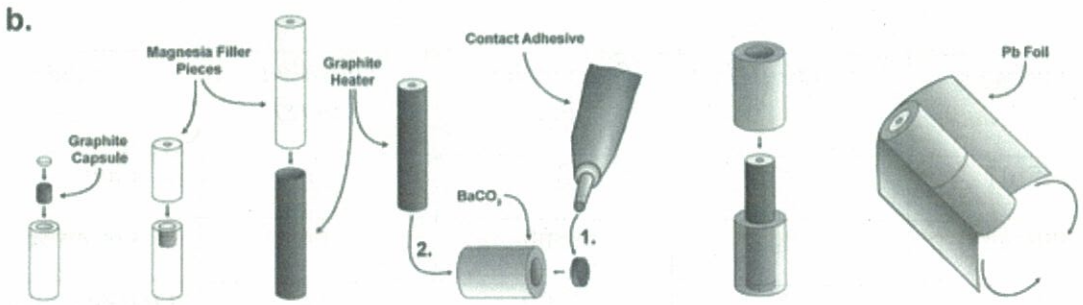


*Figure 2: Schematic of sample assembly (Bennett et al, in press).*

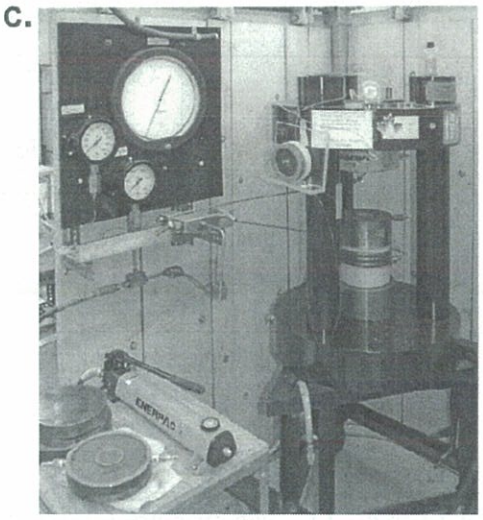


*Figure 3: Piston Cylinder apparatus (Bennett et al, in press).*

A total of 6 experiments were run at temperatures of 1300C and pressures of 2 GPa. Experiments were run at durations of 22, 67, and 120 hours. Table 1 summarizes

the specific conditions of each experiment. After completion of each experiment, the capsule was extracted and mounted in epoxy.

| *Experiment* | *Pressure (GPa)* | *Temperature (C)* | *Duration (hours)* | *Capsule* |
|---|---|---|---|---|
| PtSol1 | 2 | 1300 | 67 | Graphite |
| PtSol2 | 2 | 1300 | 22 | Graphite |
| PtSol3 | 2 | 1300 | 22 | Graphite-lined sealed Pt capsule |
| PtSol4 | 2 | 1300 | 22 | Magnetite (*hematite/Pt powder mixture) |
| PtSol5 | 2 | 1300 | 22 | Graphite-lined sealed Pt capsule |
| PtSol6 | 2 | 1300 | 120 | Graphite-lined sealed Pt capsule |

Table 1.

**Experiments at 0.1 MPa & 1000 C**

A melt composition of 50:50 mol % $CaCO_3$:$Na_2CO_3$ was prepared. This melt composition was used as it is 100% liquid at the temperature and pressure conditions used (Shatskiy, 2013).

Three experiments were done at 0.1 MPa using vacuum-sealed silica ampoules. In order to control the $fO_2$, solid metal oxide buffers were used. The metal oxide buffers have two components: oxygen and metal, i.e. $Ni(s) + \frac{1}{2}O_2(g) \leftrightarrow NiO(s)$, thus

according to the Gibbs Phase Rule the reaction is univariant. This means that the coexistence of the two phases (metal and metal oxide) at a constant temperature fixes the $fO_2$ (Fegley, 2013). The $fO_2$ of the experiment can thus be controlled by choosing the appropriate metal oxide buffer reaction.

The first run (AuSol1) of 24-hour duration used a Ni-NiO buffer. The second run of 50-hour duration was conducted with three samples using 1) Ni-NiO, 2) $Mn_2O_3$-$Mn_3O_4$, 3) Mo-$MoO_2$ buffers. The third run of 24-hour duration was conducted with three samples using 1) Co-CoO, 2) $Mn_2O_3$-$Mn_3O_4$, 3) Mo-$MoO_2$ buffers. Table 2 displays the experiment matrix for this method.

| Experiment ID | Duration | Metal | T (C) | Buffer | Log $fO_2$ |
|---|---|---|---|---|---|
| AuSol1 | 24 | Au | 1000 | Ni-NiO | -10.3 |
| Mo(1/16) | 50 | Au-Ir | 1000 | Mo-$MoO_2$ | -14.8 |
| Ni(1/16) | 50 | Au-Ir | 1000 | Ni-NiO | -10.3 |
| Mn(1/16) | 50 | Au-Ir | 1000 | $Mn_2O_3$-$Mn_3O_4$ | -6.7 |
| Mo(1/20) | 24 | Au-Ir | 1000 | Mo-$MoO_2$ | -14.8 |
| Co(1/20) | 24 | Au-Ir | 1000 | Co-CoO | -11.8 |
| Mn(1/20) | 24 | Au-Ir | 1000 | $Mn_2O_3$-$Mn_3O_4$ | -6.7 |

Table 2.

The assembly (figure 4) was prepared as follows: a 100 mg mixture of buffer was put in a silica tube, and covered with coarsely crushed silica. A small Au capsule containing a ~2.5 mm Ir wire and the prepared melt was placed on top of the crushed silica. A silica spacer was place above the Au capsule. The silica tube was then vacuum-sealed using a blowtorch, and put in a 1 atm furnace at 1000C.

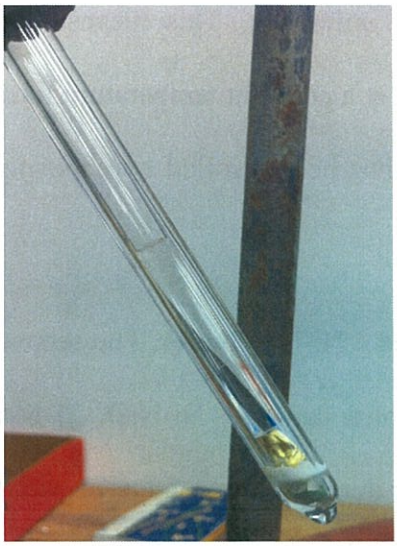

*Figure 4: Silica tube configuration: green buffer (Ni-NiO mixture), crushed silica, Au capsule and silica spacer.*

Following completion, the sample was removed and the buffers were analyzed using XRD to confirm the presence of both phases. The AuSol1 sample was mounted and analyzed using LA-ICPMS. Runs two and three were analyzed using Solution ICP-MS Standard Addition.

To prepare the sample for Solution ICP-MS an analytical method had to be developed. There were a number of problems encountered with digesting the sample and determining the correct volume of standard addition, so the methods were subject to trial and error.

First, the melt was carefully extracted from the Au capsule using a razor blade. Only large crystals of the melt were chosen for analysis, in order to prevent contamination from small Au pieces produced by cutting the capsule open. The melt crystals were weighed five times with a balance, and the average weight was calculated.

In order to yield the 1 mol/L HCl needed for the blank and rinsing solution, 8 mL of 37% high purity HCL was diluted into 100 mL of de-ionized $H_2O$. The samples were digested in 1 mol/L of HCl (~40 mg of melt in 200 mL HCl or ~20 mg of melt in 100 mL HCl). A large volume of HCl was used to digest the samples, as a white precipitate would remain if insufficient HCl was added, and also because an initial analysis using solutions with ~40 mg of melt in 100mL HCl clogged the ICP-MS lines.

Four falcon tubes were each filled with 5mL of the sample solution. A 5 ppm spike was made using a 100 ppm precious metals standard solution. The spike was added in increasing amounts to tubes 2, 3 and 4 (15 ul, 30, 50 ul, respectively). See Figure 5 for a schematic.


*Figure 5: From left to right, Mn(1/20) solution (melt from Mn 1/20 experiment dissolved in 100 mL 1 mol/L HCl); 5 ppm Au/Ir spike; 4 falcon tubes (containing 5 mL of Mn(1/20) solution, and 0 – 50 ul of 5 ppm spike); 1 mol/L HCl; Alfa Aesar 100 ppm precious metals standard solution.*

The spike volumes were chosen based on Dr. M. Gorton's advice that a maximum 1% dilution of the initial sample solution was acceptable. The four tubes and 5 mL of the blank were run on Dr. Bray's solution ICP machine in standard addition mode in order to get the Au and Ir concentration of the sample solution (unspiked sample concentration in falcon tube #1). The concentration of Au and Ir in the blank solution was measured first to control any 'background' intensity. Then after inputting the known concentrations of the added spike volumes into the software (i.e. 15 ul of a 5 ppm spike is 15 ppb, 30 ul of 5 ppm spike is 30 ppb, etc.), the concentrations of the spiked solutions were measured. This analysis creates a calibration curve, where the concentration of each spiked solution is plotted against its counts per second intensity (minus the cps of the blank). Then the unspiked sample was analyzed by looking at the x-axis intercept and the slope of the calibration curve, and based on this information the software determined the unspiked concentration of Au and Ir. Figure 6 shows the graph produced by Solution ICP-MS, the intercept is the concentration of the sample solution.

## Textural and Chemical Analysis

### Texture and Phase Chemistry of Major Elements

It is apparent through investigation with the SEM, that there is extreme phase heterogeneity, as the melt does not quench to a nice uniform texture. The lighter areas of the quenched run product are more sodium rich, while darker areas are more calcium rich. Figures 7 and 8 show the texture. The lighter areas are hypothesized to be

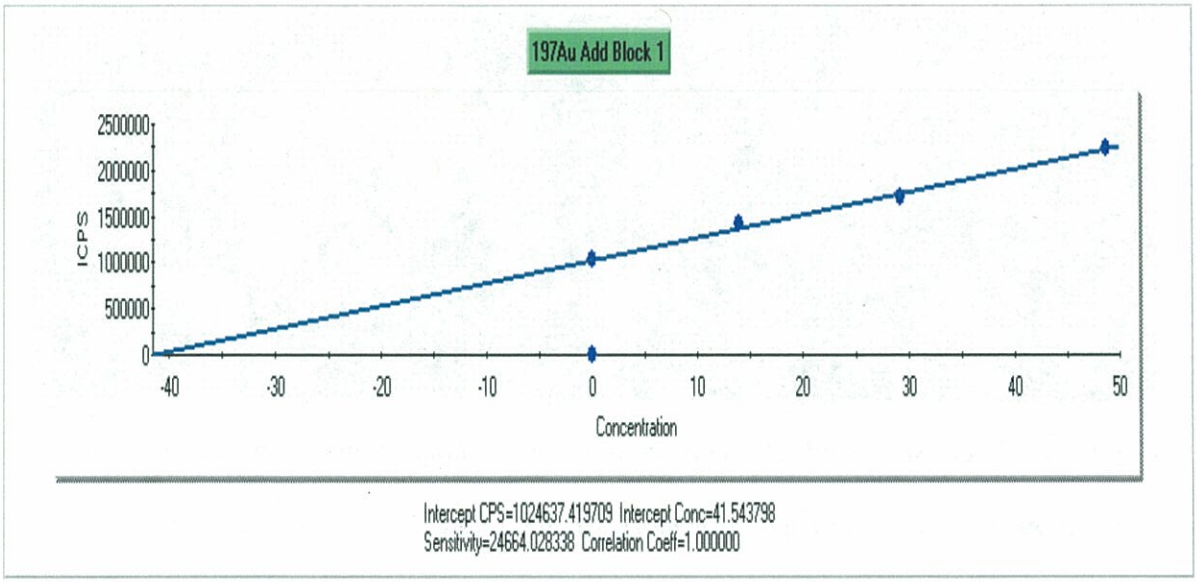


*Figure 6: Solution ICP-MS Standard Addition Graph for experiment Co(1/20). Concentration (ppb) of sample solution vs. Counts Per Second. The sample concentration for this experiment is 41.5 ppb.*

natrofairchildite ($Na_2Ca(CO_3)_2$), (1 to 1 Na:Ca ratio). Based on the relative peak heights in the EDS spectra there did not appear to be any gold in the quenched melt.

There was no difference in the chemical analysis of the major elements present in the quenched melt products between AuSol1 and the other experiments (i.e. Mo(1/20), Co(1/20), etc.). The ratios of Ca to Na were similar, and neither Au or Ir was detected. Using INCA software, the weight percents of the elements present within the sample were quantified. Oxygen accounted for 50% weight %, Na varied from 14 – 30 % wt %, and Ca varied from 15 – 40% wt %.

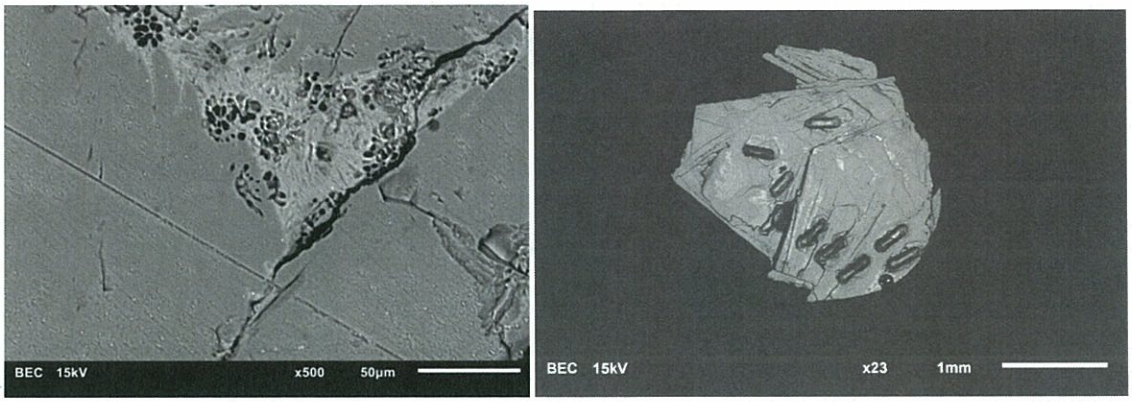


*Figure 7: Back scattered electron images of carbonate melt crystal from AuSol1 experiment. Left: Lighter areas are more Na rich and darker areas are more Ca rich. Right: It is apparent that the laser ablation marks crossed darker/lighter areas.*

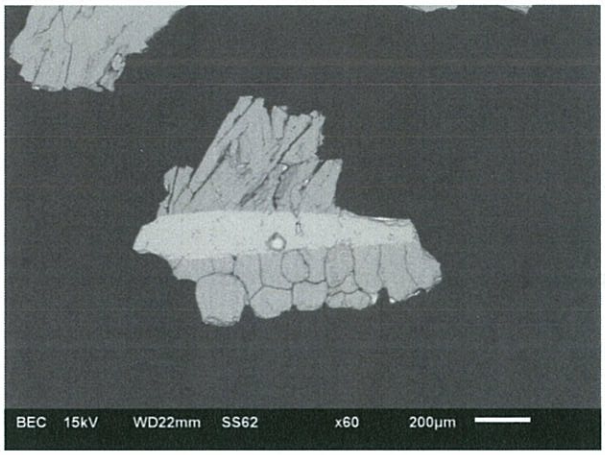


*Figure 8: Back scattered electron image of carbonate melt fragment from the 50 hour $Mn_2O_3$-$Mn_3O_4$ buffer experiment. Note the significant textural changes within the fragment. The lower portion of the fragment lacks dendritic crystals, which suggests it may have remained solid during the experiment. These textural changes were not seen in the other runs done at a lower $fO_2$.*

## Trace Element Analysis

### *LA-ICPMS*

In situ LA-ICPMS analysis produced results that were not possible to quantify due to the phase heterogeneity (see figures 7 and 8), and probable Pt contamination. A time-resolved spectrum for experiment *PtSol3* is shown in Figure 9. The varying signal indicates Pt contamination on the sample surface and/or extreme phase heterogeneity as indicated from the coarse nature of the quench (see figure 7). Carbonate melt is very soft, and when the epoxy mount was polished the Pt in the sample smeared all over the slide, causing Pt contamination. The piston cylinder experiments were thus abandoned and a new strategy for measuring solubility was pursued. Analysis by Solution ICP-MS Standard Addition was proposed as a method that could circumvent the textural heterogeneity and contamination issues.

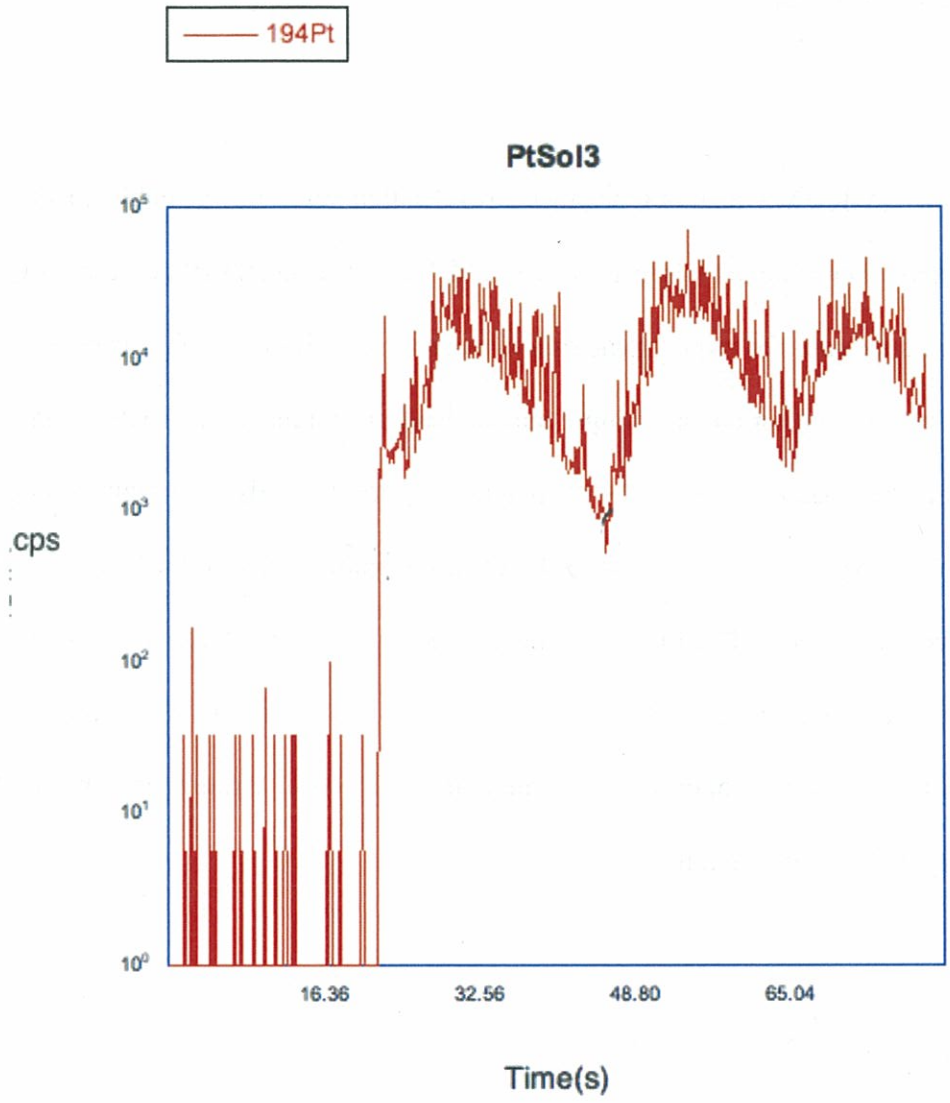


*Figure 9: LA-ICPMS time-resolved spectrum of ablation spot 3 from experiment PtSol3. The first 20s represent the gas blank, and the following 60s is the ablation signal. Note how the signal intensity varies over orders of magnitude.*

***Solution ICP-MS***

The solution ICP-MS results for the solubility of Au and Ir in carbonate melts are shown in Figures 10 and 11, respectively.

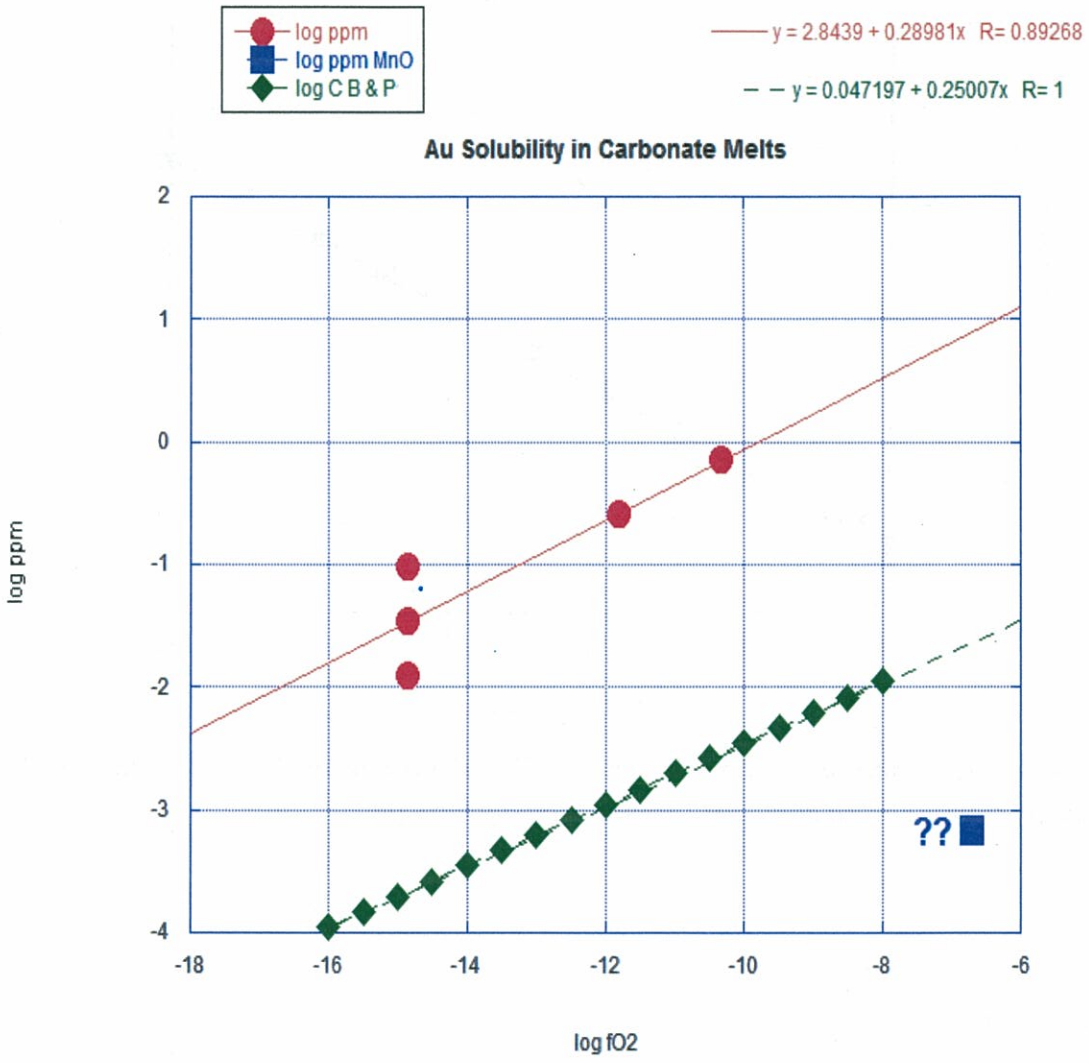


*Figure 10: Graph of Au (log ppm) vs. log $fO_2$. Results from this study (pink), from Borisov and Palme, 1996 (green), and the anomalous results for Au solubility for the $Mn_2O_3$-$Mn_3O_4$ buffer experiments (blue).*

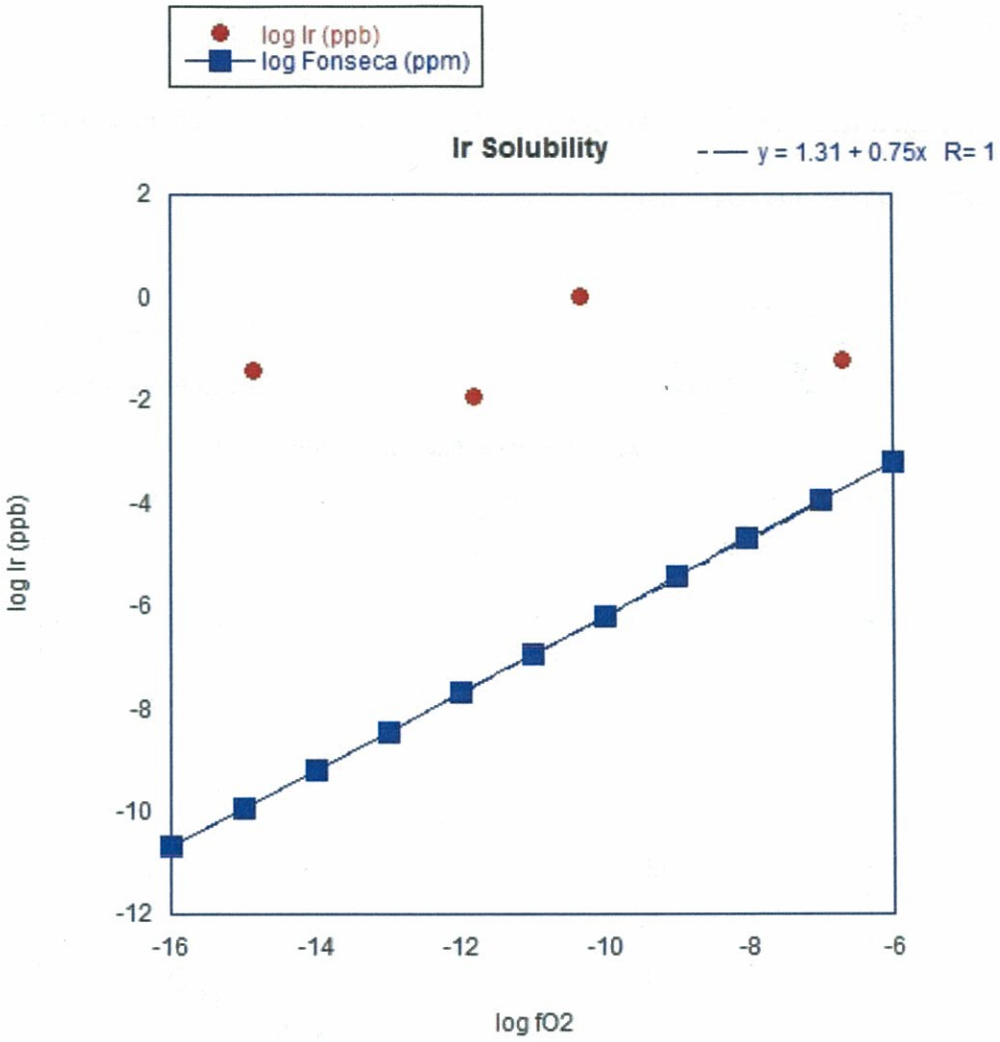


*Figure 11: Graph of Ir (log ppb) vs. log $fO_2$. Results from this study (red) in the ppb range, from Fonseca et al, 2011 (blue) in the ppm range.*

## Discussion

Figure 10 shows that Au solubility is linearly dependent on the $fO_2$ - as oxygen fugacity decreases, Au solubility also decreases. Using equation 3, the 0.28 slope of the solubility vs. log $fO_2$ trend line shows that Au probably dissolves as $Au^{+1}$. Using the equilibrium equation from O'Neill et al. (1995):

$Au_{(metal)} + x/4O_{2(gas)} \leftarrow \rightarrow AuO_{x/2(melt)}$, where x = valence of dissolved metal species (4)

the dissolved metal species in the carbonate melt from these experiments is assumed to be $Au_2O$.

While almost all the experimental results fall on the line with a slope of 0.28, the experiments run with the $Mn_2O_3$-$Mn_3O_4$ buffer did not produce Au concentrations that fell anywhere near the line. At a log $fO_2$ of -6.7 (that of the Mn buffer oxide reaction) the slope equation predicts that the solubility of Au in the melt should be 6.94 ppm. However, the experimental value is 0.69 ppb. As two runs were done using this buffer, the results were considered reproducible, and errors in the sample preparation were not considered to be the cause. Further steps were taken to investigate the anomalous result.

XRD results did not reveal any differences between the samples with the Mn oxide buffer vs. the samples with the other buffers. SEM analysis also showed the same phases in all the samples. However, there was a significant textural difference in the samples with the Mn oxide buffer that was not observed in the other runs (lack of dendritic crystals in a portion of the fragment suggesting lack of melting, see figure 8). Additionally, when the melt was extracted from the Au capsule in the silica tubes that contained the Mn oxide buffer there were not any large crystals, unlike the melt extracted from the samples containing the other buffers. Based on these observations, it is plausible that the high $fO_2$ of this buffer reaction altered the melt structure and resulted in the anomalously low Au solubility.

Au solubility in carbonate melts was compared with data from Borisov and Palme (1996). Their study experimentally determined the solubility of Au in silicate melts. In

order to compare the two datasets, the silicate melt solubility had to be extrapolated to 1000 C using their measured T dependence equation:

$$(\log (\text{Au, ppm}) = 0.25 * \log fO_2 + 2080/T + 0.59) \quad (5)$$

Figure 10 clearly indicates that Au is significantly more soluble in carbonate melts than in silicate melts. For example, at log $fO_2$ of -12, the Au ppb in carbonate melts is 232 ppb, whereas it is extrapolated to only be 1 ppb in the silicate melt. In general, Au is two orders of magnitude more soluble in carbonate melts than in silicate melts.

The solubility difference between silicate and carbonate melts may be due to the presence of many network modifying cations (like Ca) and the lack of network forming silicas in carbonate melts. Turchiaro (2013) found that the solubility of Rh and Pt increases with decreasing $SiO_2$ in the melt phase, thus a high solvation capacity is expected for a low silica melt. Farges et al. (1999) have also demonstrated that high Ca melts (like carbonatites) have significant Pt solubility, as $Ca^{2+}$ complexes with Pt. Based on their studies it is not surprising that the results from this study show that carbonate melts have a higher solvation capacity. However, as Rh and Pt are divalent and Au is monovalent at these experimental conditions, it is important to look at the behaviour of Pd in silicate melts. Pd is usually monovalent in silicate melts at most geologically relevant $fO_2$ (Borisov, 1994). While Borisov (2011) also found that Pd solubilities decreased with decreasing $fO_2$, Pd solubility increased with increasing silica content. The increase of Pd solubility with increasing silica content contrasts with the experimental Au solubility results from this study, as a low solvation capacity would be expected for a low silica melt.

While the relationship between Au solubility and $fO_2$ was clearly demonstrated, the results for the solubility of Ir in carbonate melts are inconclusive. There appears to be no relationship between the solubility and log $fO_2$ (see Figure 11). It is assumed that the concentration of Ir in the solution was below the detection limit of the ICP-MS (estimated to be 0.006 ppb)[1]. In contrast, Fonseca et al. (2011) found a clear linear relationship between Ir solubility and $fO_2$ in silicate melts, and had concentration values in the ppm range. However, these experiments were conducted at higher $fO_2$s (log $fO_2$ -6 to 1), and it could be that their slope trend line cannot be applied to the lower oxygen fugacities used in this study.

## Conclusion

These experiments demonstrate that gold is significantly more soluble in carbonate melts than in silicate melts. Many more experiments are needed to explore the relationship between highly siderophile elements and carbonatites. This study provided the stepping stone in beginning to understand how the precious metals can be mobilized by carbonatites, and if carbonatites could be an economic source for the precious metals.

[1] Estimate provided by Colin Bray via email correspondence April 6, 2015.

**References**

Bennett, N., Brenan, J.M. and Fei, Y. Metal-Silicate Partitioning Experiments at High Pressures and Temperatures: Experimental Methods and a Protocol for Suppressing Highly Siderophile Element Inclusions. Journal of Visualized Experiments, in press.

Borisov, A., and Danyushevsky, L. (2011). The effect of silica contents on Pd, Pt and Rh solubilities in silicate melts: an experimental study. European Journal of Mineralogy, 23: 355-367.

Borisov, A. and Palme, H., 1996. Experimental determination of the solubility of Au in silicate melts. Mineralogy and Petrology, 56: 297 – 312.

Borisov, A., Palme, H. & Spettel, B., 1994. Solubility of palladium in silicate melts: Implications for core formation in the Earth. Geochimica et Comoschimica Acta, 58(2): 705-716.

Dasgupta, R., and Hirschmann, M., 2006. Melting in the earth's deep upper mantle caused by carbon dioxide. Nature, 440(7084): 659-662.

Ertel, W., O'Neill, H., Sylvester, P., & Dingwell, D., 1999. Solubilities of pt and rh in a haplobasaltic silicate melt at 1300°C. *Geochimica Et Cosmochimica Acta, 63*(16), 2439-2449.

Ertel, W., O'Neill, H., Sylvester, P., Dingwell, D. and Spettel, B., 2001. The solubility of rhenium in silicate melts: Implications for the geochemical properties of rhenium at high temperatures. Geochimica et Cosmochimica Acta, 65(13): 2161–2170 .

Ertel, W., Dingwell, D. and Sylvester, P.,2008. Siderophile elements in silicate melts — A review of the mechanically assisted equilibration technique
and the nanonugget issue. Chemical Geology, 248: 119 – 139.

Farges F., Neuville D., Brown G., 1999. Structural Investigation of platinum solubility in silicate glasses. American Mineralogist. 84(10): 1562-1568.

Fegley, B., ed., 2013. Practical chemical thermodynamics for geoscientists. Amsterdam: Academic Press (Elsevier).

Fischer, T. et al., 2009. Upper-mantle volatile chemistry at Oldoinyo Lengai volcano and the origin of carbonatites. Nature, 459(7243): 77-80.

Fonseca, R., Mallmann, G., O'Neill, H., Campbell, I. and Laurenz, V., 2011. Solubility of Os and Ir in sulphide melt: Implications for Re/Os fractionation during mantle melting. Earth and Planetary Sciences: 311, 339-350.

O'Neill, H., Dingwell, D., Borisov, A., Spettel, B., & Palme, H., 1995. Experimental petrochemistry of some highly siderophile elements at high temperatures, and some implications for core formation and the mantle's early history. Chemical Geology: 120(3-4), 255-273.

Shatskiy, A. et al., 2013. New experimental data on phase relations for the system Na2CO3-CaCO3 at 6 GPa and 900–1400 °C. American Mineralogist, 98: 2164–2171.

Srivastava, R., 1997. Petrology, geochemistry and genesis of rift-related carbonatites of Ambadungar, India. Mineralogy and Petrology: 61(1-4): 47-66.

Turchiaro, F., 2013. An Experimental Study of the Solubility of Platinum (Pt) and Rhodium (Rh), with Some Results for Chromium (Cr) Content at Chromite Saturation, in Molten Basalt- Rhyolite Mixtures. MASc Thesis. Department of Earth Sciences, University of Toronto.

Wallace, M. and Green, D., 1988. An experimental determination of primary carbonatite magma composition. Nature 335: 343-346.

Xu, C. et al., 2003. PGE geochemistry of carbonatites in Maoniuping REE deposit, Sichuan Province, China: Preliminary study. Geochemical Journal, 37: 391 – 399.

Xu, C. et al., 2008. Abundances and significance of platinum group elements in carbonatites from China. Lithos 105: 201-207.